AIP | Applied Physics Letters

Non-contact thermoacoustic detection of embedded targets using airborne-capacitive micromachined ultrasonic transducers

Hao Nan, Kevin C. Boyle, Nikhil Apte, Miaad S. Aliroteh, Anshuman Bhuyan, Amin Nikoozadeh, Butrus T. Khuri-Yakub, and Amin Arbabian

Citation: Applied Physics Letters **106**, 084101 (2015); doi: 10.1063/1.4909508
View online: http://dx.doi.org/10.1063/1.4909508
View Table of Contents: http://scitation.aip.org/content/aip/journal/apl/106/8?ver=pdfcov
Published by the AIP Publishing

Non-contact thermoacoustic detection of embedded targets using airborne-capacitive micromachined ultrasonic transducers

Hao Nan,[1] Kevin C. Boyle,[1] Nikhil Apte,[2,3] Miaad S. Aliroteh,[1] Anshuman Bhuyan,[1] Amin Nikoozadeh,[1,2] Butrus T. Khuri-Yakub,[1,2] and Amin Arbabian[1]
[1]*Department of Electrical Engineering, Stanford University, Stanford, California 94305, USA*
[2]*Edward L. Ginzton Lab, Stanford University, Stanford, California 94305, USA*
[3]*Department of Mechanical Engineering, Stanford University, Stanford, California 94305, USA*

(Received 12 December 2014; accepted 6 February 2015; published online 25 February 2015)

A radio frequency (RF)/ultrasound hybrid imaging system using airborne capacitive micromachined ultrasonic transducers (CMUTs) is proposed for the remote detection of embedded objects in highly dispersive media (e.g., water, soil, and tissue). RF excitation provides permittivity contrast, and ultrasensitive airborne-ultrasound detection measures thermoacoustic-generated acoustic waves that initiate at the boundaries of the embedded target, go through the medium-air interface, and finally reach the transducer. Vented wideband CMUTs interface to 0.18 μm CMOS low-noise amplifiers to provide displacement detection sensitivity of 1.3 pm at the transducer surface. The carefully designed vented CMUT structure provides a fractional bandwidth of 3.5% utilizing the squeeze-film damping of the air in the cavity. © *2015 AIP Publishing LLC*. [http://dx.doi.org/10.1063/1.4909508]

Non-contact and remote detection of embedded or hidden objects in highly dispersive and opaque packaging, without the use of ionizing radiation, is one of the holy grails in remote sensing. This could have important applications in medical imaging, security screening, and non-destructive testing. Traditional radio frequency (RF), microwave, and optical techniques provide degraded detection capabilities in highly dispersive and lossy media. Dispersion and multi scattering decorrelate the signals from scatters, and there is a trade-off between penetration depth and resolution. X-ray methods use ionizing radiation and are therefore not safe for a variety of applications, and also could not be used for detection and identification of soft materials. Acoustic and mechanical methods require contact with the object, and often lack the contrast required to do sufficient material identification. Two-way losses in purely acoustic detection degrade signal levels too much, which makes it impractical for detection. In this work, we present a hybrid method based on the thermoacoustic (TA) effect and combine microwave excitation with non-contact airborne ultrasound detection to provide a robust solution to this long-standing challenge (Fig. 1). A detection system, as the first step toward an imaging system, is designed with (1) pulsed microwave excitation that generates absorption contrast based on dielectric properties of the embedded sample, (2) the thermoacoustic effect that generates ultrasonic waves due to minute local expansions, and (3) high sensitivity acoustic detection that could detect a minimum acoustic pressure of 240 μPa (rms) (corresponding to displacements down to 1.3 pm) at the transducer surface.

In microwave-induced TA imaging, tissue absorbs a portion of the electromagnetic energy based on dielectric properties and produces an ultrasonic wave that is then detected and used to reconstruct the image. The generation of the TA signal follows:[1–3]

$$\left(\nabla^2 - \frac{1}{v^2}\frac{\partial}{\partial t^2}\right)p(r,t) = -\frac{\beta}{C}\frac{\partial Q(r,t)}{\partial t}. \quad (1)$$

Here, $p(r,t)$ is the stress at position r and time t, v is the speed of sound, β is the thermal expansion coefficient, C is the specific heat capacity, and $Q(r,t)$ is the heating function, defined as thermal energy absorbed per unit time and unit mass. Equation (1) basically describes the generation of the pressure waves from a heat source. $Q(r,t)$ relates the electric and magnetic fields at position r and time t to the thermal energy absorbed in the sample. It is approximately proportional to the square amplitude of the electric field.[4,5]

TA detection combines the high dielectric contrast of microwave imaging with the resolution of ultrasound imaging.[6–8] We apply these advantages to complete non-contact detection of embedded/hidden targets. Here, the main challenge is the ability to receive ultrasound waves generated deep within the object using airborne transducers outside and at a distance (i.e., no coupling medium). In this paper, we will focus on the detection of objects embedded in the body. Pressures generated in the body will experience a large acoustic impedance mismatch when passing through the body/air interface. Taking the acoustic impedance of the body to be similar to that of water, the acoustic transmission coefficient of a water/air interface is

$$T = 1 - \frac{Z_{air} - Z_{water}}{Z_{air} + Z_{water}} = 5.4 \times 10^{-4} = -65.4\text{dB}. \quad (2)$$

Here, acoustic impedance is defined as $Z = \rho c$, where ρ is the density of the medium and c is the speed of sound in that medium. For air ($\rho = 1.2\,\text{kg/cm}^3$ and $c = 343\,\text{m/s}$), $Z = 408$ Rayl and for water ($\rho = 1000\,\text{kg/cm}^3$ and $c = 1482\,\text{m/s}$), $Z = 1.48 \times 10^6$ Rayl.[9]

The sensitivity of the sensor and electronics is critical in enabling detection at a standoff. The main sensitivity figure of merit is the minimum detectable pressure or surface displacement at the surface of the receiving transducer, which determines the minimum detectable signal level coming from the embedded target after the acoustic signal goes through the 65 dB interface loss. As a first order

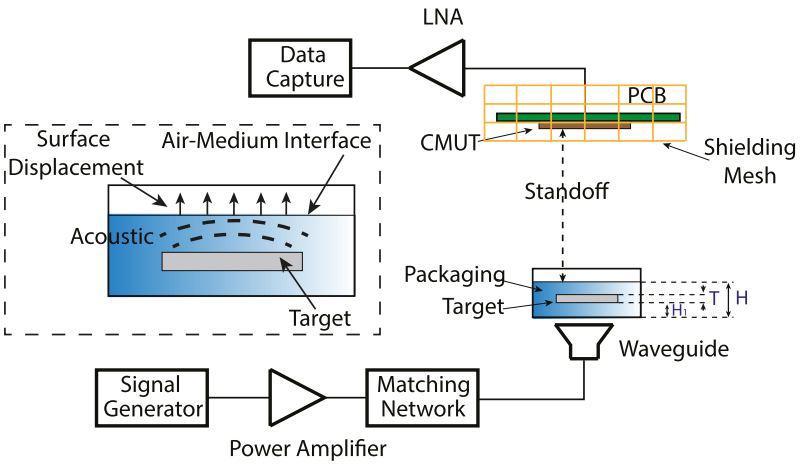

FIG. 1. Schematic of the non-contact thermoacoustic detection setup. H is the thickness of packaging material (medium) (set between 1 and 3 cm of water or Agarose). T is the thickness of embedded target (e.g., Rexolite, set to 4 mm layers and target area of 4 cm^2).

approximation, 1 mK of heating results in 800 Pa pressure,[10] and this can be used to model the required local Specific Absorption Rate (SAR) and resulting thermoacoustic generated pressure that arrives at the medium-air interface. Additionally, larger bandwidth (BW) is required for time-gating and accurate time-of-flight measurements in the proposed imaging/detection method. In general, higher bandwidth in the detector allows a shorter time domain response to an incoming TA signal and a correspondingly higher resolution. However, some sensitivity is lost with the larger bandwidth and must be traded off with resolution appropriately, considering the 65 dB loss of signal at water/air interface.

Here, we use capacitive micromachined ultrasonic transducers (CMUTs) as our ultrasound sensors, as shown in Fig. 2. CMUTs use thin vibrating plates for generating and detecting ultrasound. CMUTs have excellent impedance match with air due to the low mechanical impedance of these thin plates. Hence, they are ideal for ultrasound detection in air.[11,12] By applying a large enough DC electric field between the two electrodes of the CMUT, it is possible to get a high electromechanical coupling coefficient approaching unity.[13] Typically, the gap between the CMUT plate and the substrate is evacuated. However, for this application, we designed CMUTs with the gap vented to the ambient air. The squeeze film energy loss from the air in the cavity as well as viscous and thermal energy losses from the air in the venting holes

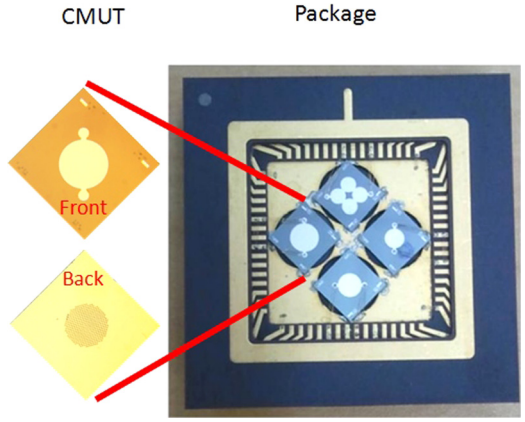

FIG. 2. The packaged CMUTs used in the experiments with a detail view of the front and back of one device. The back side shows the venting holes.

helps to increase the bandwidth of the CMUT at the expense of some sensitivity.[14] By carefully engineering the location, size, and the number of vent holes, we can optimize the CMUT sensitivity as well as bandwidth. We designed and fabricated CMUTs vented either through the CMUT plate or through the substrate. The CMUTs were made with a wide range of bandwidth from 3% to 30% and with resonant frequency ranging from 70 kHz to 170 kHz. Fig. 3 shows the displacement measurement for one such CMUT using a Laser Doppler Vibrometer (LDV) as well as pitch-catch measurement for a pair of CMUTs of this design. These CMUTs have a resonant frequency of 72 kHz and a fractional bandwidth of 3.5%.

To perform accurate sensitivity measurements, a calibrated commercial microphone (G.R.A.S. 40DP 1/8″) was used to measure the pressure generated at a set standoff distance from a CMUT configured to transmit ultrasound at 72 kHz. The calibrated microphone was then replaced with the receiver CMUT, as shown in Fig. 3, and the results of this pitch-catch setup were used with the calibrated pressure results to determine the pressure sensitivity of the CMUT. A minimum detectable pressure at the face of the CMUT of 240 μPa (rms) was achieved along with a recorded sensitivity of 6.4 V/Pa for the CMUT and on-board low-noise amplifier (LNA). This pressure is equivalent to a minimum detectable displacement at the face of the CMUT of 1.3 pm, given by $p = 2\pi \times f \times Z \times x$, where p is pressure, f is the ultrasound frequency, Z is the acoustic impedance of the medium, and x is the displacement. We are now only 6 dB away from the theoretical mechanical noise floor with the custom CMUT. Further improvement can be achieved by later generations of the LNA.

To determine the minimum detectable pressure and displacement at the target surface using the characterized CMUT, we must consider diffraction and propagation losses. At a standoff distance of $z = 30$ cm from a target with radius $a = 2$ cm, propagation losses were calculated with the Fresnel approximation where

$$\frac{p(z)}{p(0)} = \sqrt{4\sin^2\left(\frac{\pi}{2S}\right)} = -1.11\text{dB}. \tag{3}$$

The Fresnel parameter $S = (z \times \lambda)/a^2$ with $\lambda = 4.6$ mm corresponding to the 72 kHz CMUT. Taking into account this

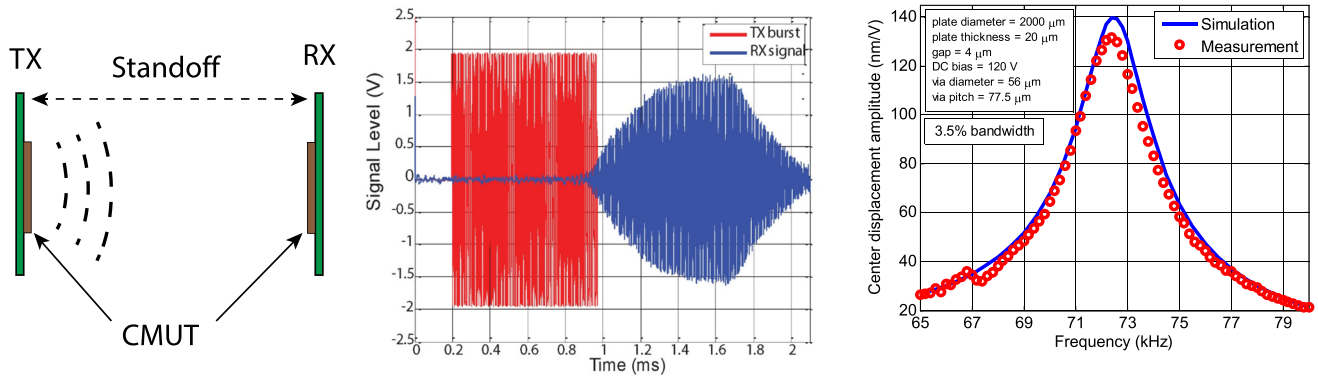

FIG. 3. Pitch-catch experiment setup used for the sensitivity and bandwidth characterization of CMUTs. LDV measurements (right) show the TX CMUT displacement and frequency response. Finite Element Analysis simulations are performed for modeling and the results match measurements. The minimal detectable pressure of RX CMUT is 240 μPa (rms) when measured with the calibrated microphone pitch-catch experiment.

propagation loss, the minimum detectable pressure at the CMUT of 240 μPa (rms) corresponds to a minimum detectable pressure at the air-medium interface (Fig. 1) of 272 μPa (rms) and minimum detectable surface displacement of 1.5 pm.

The standard measurement setup is shown in Fig. 1. The envelope of the 2.4 GHz RF signal from a high-power power amplifier (PA) is modulated with N ($=10$–40) cycles of on-off keying (OOK) bursts at 72 kHz with a 50% duty cycle. This whole sequence repeats with repetition interval of 10–20 ms. A matching network interfaces the PA to the open-face waveguide that excites the sample from the bottom or the sides. The CMUT receiver is placed at a standoff distance of approximately 30 cm above the target (e.g., 4 mm thick Rexolite embedded in Agarose, chosen to provide dielectric contrast with water).[15] The CMUT and printed circuit board (PCB) are enclosed in a copper mesh cage to provide RF shielding from both the RF source and the environment. The shield presents 0.7 dB acoustic loss at 72 kHz. Measurements were performed both with and without an RF enclosure around the target to direct RF power. Here, we present results from target samples of hidden Rexolite within either water or Agarose.

The system achieves an end-to-end signal-to-noise ratio (SNR) of 36 dB (with $N_{avg} = 100$ and an average RF power of 13.8 W) to detect 4 mm Rexolite layers embedded in 1–3 cm of high water content Agarose at a 30 cm standoff. In order to verify the received signals were from the expected interface, we used both time of flight calculations as well as simulations of the expected signal given the measured frequency characteristics of the CMUT. Fig. 4 shows the results for an embedded rexolite target in different media with and without the RF enclosure. Ultrasound echoes and other clutter are visible in the high SNR plot and are the result of the physical setup of the experiment.

To first order, we can approximate the differential instantaneous temperature change in the sample needed to create the thermoacoustic signal measured at the CMUT in our experiments. Fig. 4(a) shows a received signal of 18 mV(pk-pk) or 2.5 mPa at the face of the CMUT given the recorded sensitivity, which includes the gain of the LNA. Taking into account the 1.11 dB propagation loss and 65 dB impedance mismatch at the surface of the medium, the pressure at the target surface must be 5.05 Pa to result in the measured signal. Using the 1 mK per 800 Pa relationship discussed earlier, this translates to an approximate differential heating of 6.3 μK at the surface of the target to generate the signal recorded in our experiment.

This imaging system achieves remote interrogation of highly dispersive media for deeply embedded abnormalities. With a CMUT displacement sensitivity of 1.3 pm at the transducer surface, the system is able to detect 4 cm^2 embedded targets from a standoff distance of 30 cm. This performance could enable a myriad of applications including medical imaging applications, security screening, and non-destructive testing. Further work will investigate higher

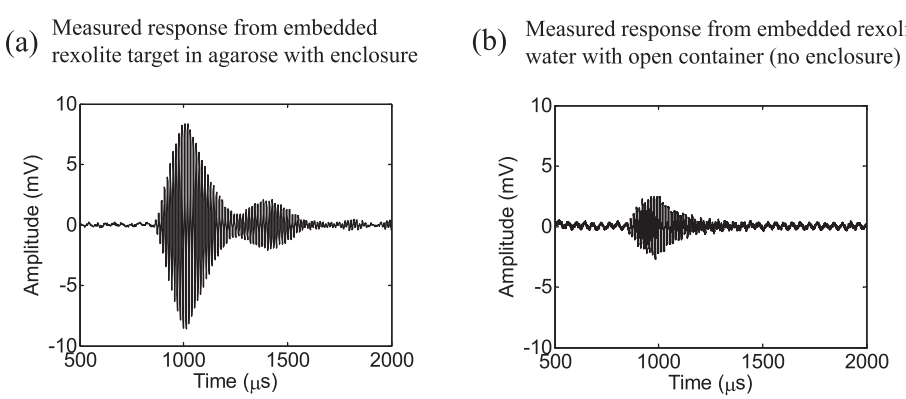

FIG. 4. (a) Detection of embedded 4 mm Rexolite layers with the enclosure showing 36 dB SNR. (b) Detection of embedded 4 mm Rexolite layers in water without the enclosure.

bandwidth and multi-frequency devices to increase resolution, while balancing tradeoffs such as penetration depth through tissue and obstruction layers.

The authors acknowledge Rohde and Schwarz, RFMD, support from the DARPA MEDS program and Stanford CIS seed grant, and chip fabrication by Texas Instruments. Special thanks to Dr. Nemat Dolatsha for valuable comments and suggestions.

[1]M. W. Sigrist, J. Appl. Phys. **60**, R83 (1986).
[2]X. Feng, F. Gao, and Y. Zheng, Appl. Phys. Lett. **103**, 083704 (2013).
[3]C. G. Lou, S. H. Yang, Z. Ji, Q. Chen, and D. Xing, Phys. Rev. Lett. **109**, 218101 (2012).
[4]H. Nan and A. Arbabian, Appl. Phys. Lett. **104**, 224104 (2014).
[5]D. Razansky, S. Kellnberger, and V. Ntziachristos, Med. Phys. **37**, 4602–4607 (2010).
[6]G. Ku and L. V. Wang, Med. Phys. **27**(5), 1195–1202 (2000).
[7]F. Gao, Q. Zheng, and Y. Zheng, Med. Phys. **41**, 053302 (2014).
[8]S. Kellnberger, M. Omar, G. Sergiadis, and V. Ntziachristos, Appl. Phys. Lett. **103**, 153706 (2013).
[9]P. Filippi, D. Habault, J.-P. Lefebvre, and A. Bergassoli, *Acoustic: Basic Physics, Theory, and Methods* (Academic Press, San Diego, 1999), p. 33.
[10]L. V. Wang, Nat. Photonics **3**(9), 503–509 (2009).
[11]A. Bhuyan, J. W. Choe, B. C. Lee, I. Wygant, A. Nikoozadeh, O. Oralkan, and B. T. Khuri-Yakub, ISSCC Dig. Tech. Pap. **2013**, 396–398.
[12]M. N. Senlik, S. Olcum, H. Köymen, and A. Atalar, in *Proceedings of IEEE International Ultrasonics Symposium* (2009), pp. 438–441.
[13]G. G. Yaralioglu, A. S. Ergun, B. Bayram, E. Hæggström, and B. T. Khuri-Yakub, IEEE Trans. Ultrason. Ferroelectr. Freq. Control **50**(4), 449–456 (2003).
[14]N. Apte, K. K. Park, A. Nikoozadeh, and B. T. Khuri-Yakub, in *Proceedings of IEEE International Ultrasonics Symposium* (2014), pp. 166–169.
[15]Y. Qin, P. Ingram, X. Wang, T. Qin, H. Xin, and R. S. Witte, in *Proceedings of IEEE International Ultrasonics Symposium* (2014), pp. 1033–1036.